14.1

VORTEX SHEETS, VORTEX RINGS, AND A MESOCYCLONE

David S. Nolan*
Division of Meteorology and Physical Oceanography
Rosenstiel School of Marine and Atmospheric Science
University of Miami, Miami, Florida

1. INTRODUCTION

The formation of long-lived, rotating thunderstorms is one of the more remarkable natural phenomena in the atmosphere, and it is usually a necessary first step toward the formation of significant tornadoes. It is now widely accepted that the initial devlopment of vertical vorticity and rotation in these thunderstorm updrafts is caused by the tilting of horizontal vorticity associated with low-level wind shear (Klemp 1987). When the environmental wind shear is unidirectional, the generation of vertical vorticity is symmetric about the shear vector, and two symmetric rotating storms are generated. However, it is much more often the case that the wind vector turns clockwise with height (in the northern hemisphere), leading to preferred intensification of the cyclonic storm.

This preferred intensification of the cyclonic updraft has been identified with asymmetric pressure perturbations generated by the interactions of the cyclonic and anticyclonic mesocyclones with the environmental flow (Rotunno and Klemp 1982, Weisman and Klemp 1984). Grasso (2000) showed that cooling of low-level air feeding into the left-mover by the downshear precipitation of the right-mover also has a significant effect, and that left-moving storms could continue if this effect were removed. In this study, we will neglect all moist processes and consider only the essentially nonlinear mechanism of interactions between low-level vortex lines as they are tilted and stretched into the updraft.

Vortex methods are an alternative to the traditional approach of simulating vortex dynamics with Eulerian grids. They can be particularly useful when the phenomenon of interest is essentially inviscid and evolves over short times (e.g., Nolan 2001). This presentation has two purposes: first, to demonstrate the use of 3D vortex methods for atmospheric phenomena, and second, to show how the cyclonic and anticyclonic updraft asymmetries can arise solely from vortex dynamics.

2. THREE DIMENSIONAL VORTEX METHODS FOR INCOMPRESSIBLE FLOW

In two dimensions, vortex methods simulate the evolution of incompressible flow by computing the trajectories of localized vortices in the plane (Chorin 1973, 1996). Since vorticity is conserved in two dimensional flows, the vortex strengths do not change in time, and each vortex moves according to the local velocity field induced by all the other vortices. An important result from studies of the convergence of vortex methods is that results are much more accurate when the vorticity associated with each element is smooth, i.e., "blob" methods are much more accurate than "point vortex" methods. In fact, the rate of convergence, defined as the rate at which the vortex solution approaches the "truth" as the number N of vortex elements increases, is strongly dependent of the distribution on the vorticity within the blob (Hald 1979, 1987).

Extending these ideas to three dimensions, we represent the vorticity field with a collection of vortex tubes, each of which has a vorticity distribution in its core that is smooth and has a finite cut-off radius (Leonard 1985; Knio and Ghoniem 1990). The center axis of each vortex tube is represented by a continuos chain of segments, each of which is the straight line between its endpoints $\mathbf{x}_j$ and $\mathbf{x}_{j+1}$. The familiar ideas that vortex lines are material curves in the flow, and must not end in the fluid, require that the endpoints move with the flow and individual vortex tubes remain connected at all times.

For a smooth vorticity field $\omega(\mathbf{x})$ in an unbounded domain, a vector potential ϕ may be found with the use of the Green's function for the Laplace equation:

$$\phi(\mathbf{x}) = \int_{R^3} \frac{\omega(\mathbf{x}')}{4\pi|\mathbf{x}-\mathbf{x}'|} dx' \tag{1}$$

with the associated velocity field

$$\mathbf{u}(\mathbf{x}) = \nabla\times\phi = -\int_{R^3} \frac{(\mathbf{x}-\mathbf{x}')\times\omega(\mathbf{x}')}{4\pi|\mathbf{x}-\mathbf{x}'|^3} d\mathbf{x}' \ . \tag{2}$$

In the practice of vortex methods, (2) is replaced by a summation over all the vortex segments of all the tubes, with the incorporation of a smoothing function $f(r)$which is related to the vorticity distribution $g(r)$ in the core of the vortex tube by $f'(r) = 4\pi r^2 g(r)$.The velocity field may then be written

$$\mathbf{u}(\mathbf{x}) = -\frac{1}{4\pi}\sum_j \Gamma_j \frac{(\mathbf{x}_j^c-\mathbf{x})\times(\Delta\mathbf{x}_j)}{\left|\mathbf{x}_j^c-\mathbf{x}\right|^3} f\left(\frac{\left|\mathbf{x}_j^c-\mathbf{x}\right|}{\delta}\right), \tag{3}$$

where Γ_j is the circulation (strength) of each segment (constant for each individual filament), $\mathbf{x}_j^c$ is the midpoint of each segment, $\Delta\mathbf{x}_j$ is the vector connecting its endpoints, and δ is the cutoff radius of the internal vorticity distribution. The simulations presented here use

$$f(r) = 1 - e^{-r^3}, \tag{4}$$

and its associated vorticity core function

$$g(r) = \frac{3}{4\pi} e^{-r^3}, \tag{5}$$

which are known to allow for second-order convergence (Beale and Majda 1985). The evolution of the vortex lines is described by the nonlinear dynamical system

* Corresponding author address: Prof. David S. Nolan, RSMAS/MPO, 4600 Rickenbacker Causeway, Miami, FL 33149. email: dnolan@rsmas.miami.edu

$$\frac{d\mathbf{x}_j}{dt} = \mathbf{u}(\mathbf{x}_j, t) \qquad (6)$$

which we integrate in time with a fourth order Runge-Kutta scheme. As the vortex lines evolve, they will (usually) stretch and the segments will become longer. To achieve accuracy in the self-induced motion of curved vortex lines, it is critical that the lengths of the segments remain smaller than their cutoff radii (Wang 1996). Thus, if a segment becomes longer than its cutoff radius, we replace it with two segments by adding a new point in between its endpoints using a cubic interpolation scheme. A type of Courant-Lewy-Friedrichs (CFL) condition must also be maintained, such that no vortex element moves farther than its own length in one time step.

Perhaps the most common misunderstanding about vortex methods is the confusion between physical vortices and numerical vortex elements. Unlike a physical vortex, the cores of the vortex tubes described above do not change size or shape as they are advected by the flow. Rather, a physical vortex must be represented by a collection of numerical vortices, and accuracy is achieved with a good density of overlapping numerical vortices. The collective motions of these numerical elements will then properly represent the evolution of the smoothly varying vorticity field.

3. IDEALIZED REPRESENTATIONS OF LOW-LEVEL SHEAR ZONES AND UPDRFATS

Vertical wind shear is associated with horizontal vorticity; if a flow is zonal with u=$u(z)$, then the vorticity vector is oriented in the meridional direction, with value $\eta = \partial u / \partial z$. A region of vertical wind shear can then be represented as a collection of smoothed vortex sheets, such that the vorticity contribution to each point from all the nearby sheets is equal to the desired horizontal vorticity. In turn, each vortex sheet can be approximated by a collection of smoothed vortex lines, which are made up of connected vortex elements as described above.

As a crude approximation to a low-level shear zone, we use two vortex sheets at altitudes of 500 and 1000 m, each of which is described by 20 vortex lines in the region $-4000 \le x \le 4000$. Each line extends from y = -4000 to y = + 4000, consisting of 16 segments of 500 m length each. The width δ of each element are 550 m, ensuring significant overlap between the lines.

The flow is doubly periodic in the x and y directions, with a free-slip lower surface at z = 0. These boundary conditions are generated through the use of image vortices. Above the surface, each vortex element has 8 image vortices at x = -8000, 0, +8000 m, and y = -8000, 0 , +8000 m. In addition, there are image vortices below the surface, of opposite sign, for the original vortex element and each of its 8 periodic images. In the absence of additional forcing, the sheets propagate westward with the mean flow $u(z)$. We found that all 17 images were necessary to satisfactorily reproduce doubly periodic flow, such that the edges of the sheets remain square and parallel to the surface.

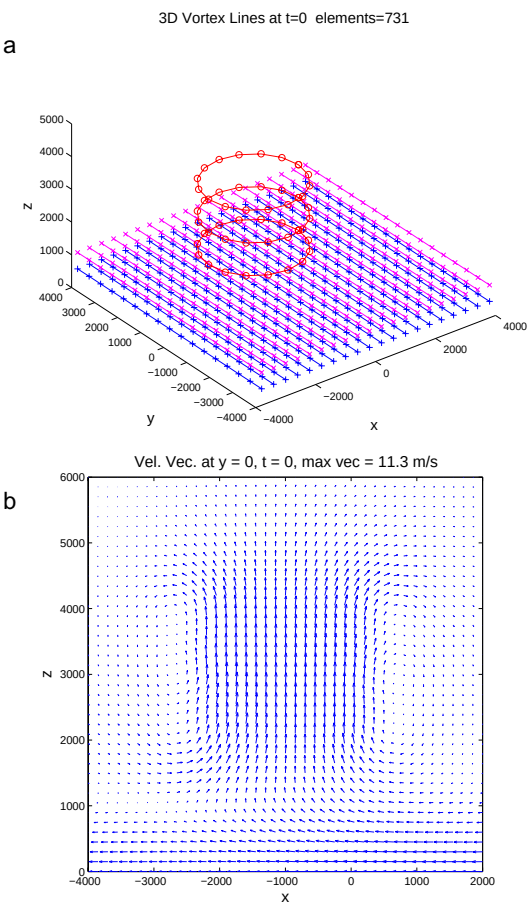

Figure 1: Initial conditions for the unidirectional shear case: a) Vortex lines. Segment endpoints are indicated by the +'s for the lower vortex sheet, x's for the upper sheet, and o's for the rings. b) Velocity vectors in the x-z plane.

We use vortex *rings* to represent a convecting updraft. A vortex ring induces a flow parallel to its axis. The rings are arranged above the center of the low-level sheets so as to induce vertical motion up from the surface. Three vortex rings of equal strength and radius 1500 m are located at x = -1000 m, y = 0, and z = 2000, 3000, and 4000 m altitude. Real vortex rings propagate in the direction of the flow they generate; however, to maintain the interaction between the updraft and the low-level flow, we hold the altitudes of vortex rings fixed. Rings of vorticity around the updraft are in fact generated by latent heat release in the full equations.

Figure 1 shows the initial condition for a unidirectional shear case. The upper plot shows the actual vortex lines used to construct the flow. The lower figure shows a vertical cross section of velocity vectors in the x-z plane. The low level wind has a shear of approximately 10 ms^{-1} in the lowest 1 km, while the updraft velocities reach 11 ms^{-1} at z = 3000 m.

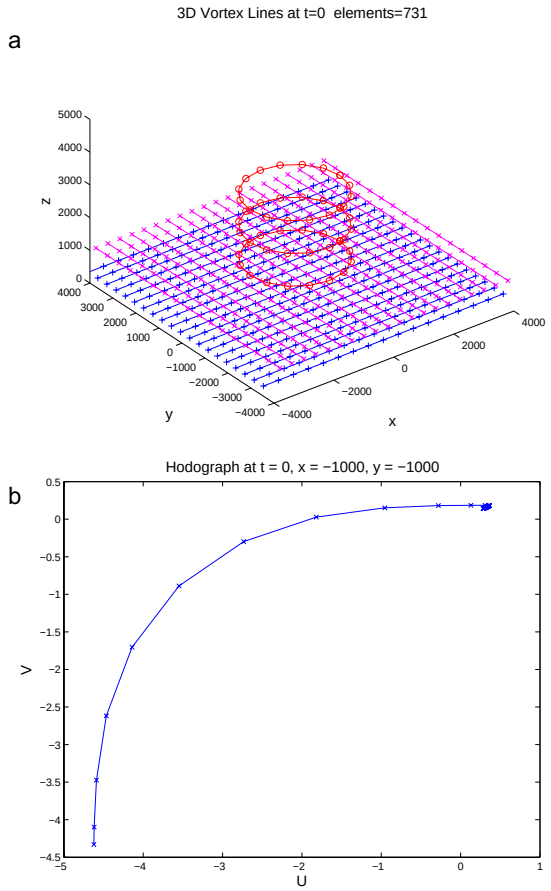

Figure 2: Initial conditions for the clockwise shear case: a) Vortex lines, as in Figure 1; b) Hodograph, with x's marking 150 m altitude increments, with the surface wind in the lower left corner.

A simple way to initialize the flow with a shear vector that rotates clockwise with height is to have the two vortex sheets oriented perpendicular to each other, as shown in Figure 2, along with the resulting hodograph. With the addition of a constant flow vector, one could recover something like a quarter-circle hodograph. As the sheets propagate southward as well as westward, the ring centers are shifted to y = -1000 m for this case.

4. EVOLUTION AND UPDRAFT ASYMMETRIES

As time evolves, the updraft advects the low-level vortex lines, tilting and stretching them as they rise. For the unidirectional shear case, the vortex lines and their associated flow fields are perfectly symmetric about y = 0, with the vortex lines bowing upward and evenutally through the vortex rings. The vortex lines at t = 480 s are shown in Figure 3a. Horizontal cross sections through the flow fields at low levels reveal an updraft pattern which is symmetric about y = 0, with two local vertical velocity maxima associated with the dynamic pressure forces of the intensifying cyclones (not shown). The vertical vorticity pattern is exactly asymmetric about y = 0 (not shown).

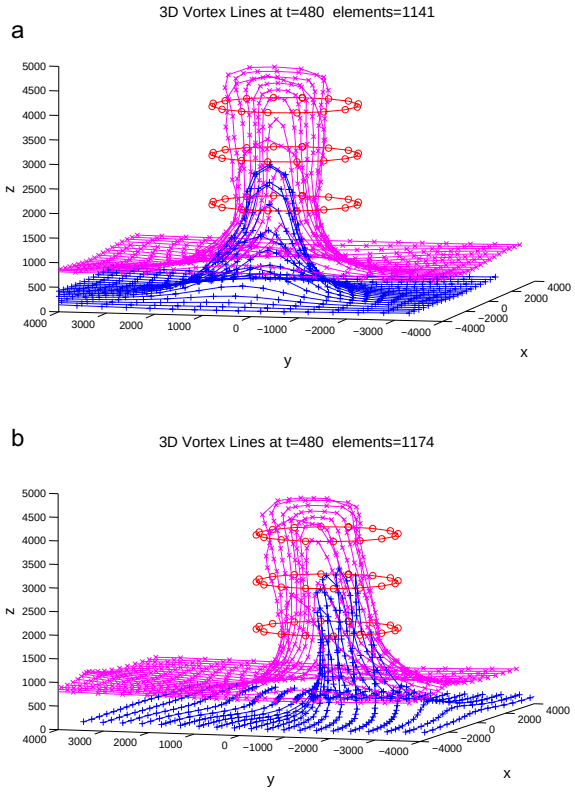

Figure 3: Vortex lines at t = 480 s, for a) the unidirectional shear case; and b) the clockwise shear case.

In the clockwise shear case, the evolution of the vortex lines becomes asymmetric, even with respect to the mean horizontal flow (to the "southwest"). The deformation of the vortex sheets occurs so that the vortex lines with positive vertical vorticity from the two different sheets become more closely aligned, while the opposite is true for the lines with negative vertical vorticity. This can be seen to some extent in Figure 3b, but it is difficult to visualize without animations or manual reorientation of the figures.

The formation of the "mesocyclones" is asymmetric, with stronger vertical velocities and vertical vorticities in the cyclonic vortex, as shown in Figure 4. The asymmetries are not great, with vertical velocity about 25% larger and vertical vorticity only slightly larger in the cyclonic updraft. At this stage, the vertical vorticity values are already more than 50% larger than the horizontal values. At lower altitudes, the vorticity asymmetry is larger, while the velocity asymmetry is smaller. Thus we have shown how asymmetric mesocyclones can develop purely from vortex dynamics in incompressible flow.

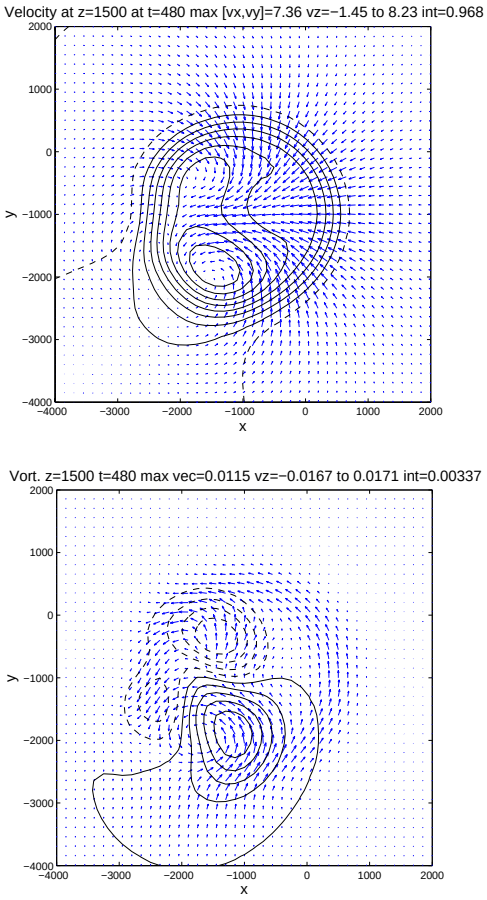

Figure 4: Horizontal cross sections of (a) velocity and (b) vorticity at t = 480 s, z = 1500 m. Contours indicate values perpendicular to the x-y plane, and vectors indicate values parallel to the plane.

5. FUTURE WORK

The results shown here are highly preliminary, as the number of vortex lines and vortex elements are probably much too small to accurately represent the details of the smoothly varying vorticity in the low-level shear region. We have illustrated the interaction of vortex lines, whose initial directions vary with height, as they are advected upward from the surface. These interactions lead to significant asymmetries in the "mesocylones" that are initially generated. In a real, moist, convecting atmosphere, these asymmetries would be amplified by nonlinear feedbacks caused by latent heat release. In future work, we will repeat these calculations with more sheets, rings, and vortex elements. We will also attempt to model the effects of downdrafts, which has been hypothesized to bring vorticity down to the surface, perhaps as a necessary triggger for tornadogenesis.

It has not been our intent to show that 3D vortex methods can replace storm-scale modeling of the atmosphere; rather, we have identified a particular short-term phenomenon that can be studied in this manner. Ultimately, the greatest contribution of this technique may be as an educational tool illustrating the tilting, stretching, and nonlinear interactions of vortex lines.

ACKNOWLEDGEMENTS:

The author would like to thank Alexandre Chorin and David Adalsteinsson for their assistance in the development of the 3D vortex model, and Dan Hodyss for his comments on this document. Some of the calculations presented here were performed while the author was a visitor at the Department of Mathematics in the Computing Science Directorate of the Lawrence Berkeley National Laboratory, in the summer of 2004; otherwise support was provided by the University of Miami.

REFERENCES:

Beale, J. T., and A. J. Majda, 1985: High order accurate vortex methods with explicit velocity kernels. *J. Comp. Phys.*, **58**, 188-208.

Chorin, A. J., 1973: Numerical study of slightly viscous flow. *J. Fluid Mech.*, **57**, 785-796.

Chorin, A. J., 1996: Vortex methods. In *Computational Fluid Dynamics*, edited by M. Lesiuer et al., Elsevier, New York.

Hald, O. H., 1979: Convergence of vortex methods for Euler's equations, II. *SIAM J. Numer. Anal.*, **16**, 726-755.

Hald, O. H., 1987: Convergence of vortex methods for Euler's equations, III. *SIAM J. Numer. Anal.*, **16**, 726-755.

Klemp, J. B., 1987: Dynamics of tornadic thunderstorms. *Ann. Rev. Fluid Mech.*, **19**, 362-402.

Knio, O. M., and A. F. Ghoniem, 1990: Three dimensional vortex methods. *J. Comp. Phys.*, **86**, 75-106.

Leonard, A., 1985: Computing three-dimensional incompressible flows with vortex filaments. *Ann. Rev. Fluid Mech.*, **17**, 523-559.

Nolan, D. S., 2001: The stabilizing effects of axial stretching on turbulent vortex dynamics. *Phys. Fluids*, **13**, 1724-1738.

Rotunno, R., and J. B. Klemp, 1982: The influence of shear-induced pressure gradients on thundestorm motion. *Mon. Wea. Rev.*, **110**, 135-151.

Wang, 1996: *A study of short wave instability on vortex filaments*. Ph.D. Thesis, Department of Mathematics, UC Berkeley.

Weisman, M. L., and J. B. Klemp, 1984: The structure and classification of numerically simulated convective storms in directionally varying wind shear. *Mon. Wea. Rev.*, **112**, 2479-2498.